FISEVIER

Contents lists available at ScienceDirect

# Scripta Materialia

journal homepage: www.elsevier.com/locate/scriptamat



## Radiation-resistant nanotwinned austenitic stainless steel

G. Meric de Bellefon <sup>a,\*</sup>, I.M. Robertson <sup>b</sup>, T.R. Allen <sup>a</sup>, J.-C. van Duysen <sup>c,d</sup>, K. Sridharan <sup>a,b</sup>

- <sup>a</sup> Department of Engineering Physics, University of Wisconsin, Madison, USA
- <sup>b</sup> Department of Materials Sciences, University of Wisconsin, Madison, USA
- <sup>c</sup> Department of Nuclear Engineering, University of Tennessee, Knoxville, USA
- <sup>d</sup> EDF—Centre de Recherche des Renardieres, Moret sur Loing, France

#### ARTICLE INFO

Article history:
Received 21 August 2018
Received in revised form 13 September 2018
Accepted 16 September 2018
Available online xxxx

Keywords: Austenitic stainless steel Nanotwinned Irradiation Deformation twinning Void swelling

#### ABSTRACT

A key strategy to increase the radiation resistance of materials has been to introduce a high density of interfaces that can act as sinks for radiation-induced defects. Twin boundaries are a type of interface that can be introduced through deformation but are usually considered to be ineffective sinks. Using heavy ion irradiation and transmission electron microscopy, this study investigates the influence of a high area per unit volume of twin boundaries on the radiation-induced swelling response of an austenitic stainless steel. The study shows that swelling can be suppressed in regions containing a high density of closely-spaced deformation twin boundaries.

© 2018 Acta Materialia Inc. Published by Elsevier Ltd. All rights reserved.

Under neutron irradiation, metals and alloys can undergo various types of structural changes at micro- and nanometer length scales [1]. At high doses (>10 dpa, displacements per atom) and at temperatures between 300 °C and 700 °C, one of these changes is void formation, which can lead to macroscopic swelling of tens of percent [2–4]. More than a few percent of swelling is typically incompatible with the demands of structural components in nuclear systems [5]. One avenue to develop swelling-resistant materials relies on the introduction of a high density of sinks for mobile point defects [5,6]. Increased sink strengths have been achieved in materials with high surface-to-volume ratios of interface sinks such as multilayered Cu-Nb composites [7–9].

Austenitic stainless steels (SS) are attractive for nuclear reactor applications [5,10] but can be prone to void swelling [11]. Tangled dislocations introduced by cold-work [12] can act as sinks and have been shown to reduce swelling in SS [13–15,4]. However, after a threshold dose of about 30 dpa for cold-worked SS to about 50 dpa for coldworked Ti-modified SS, swelling rates increase and become more similar to the ones of annealed SS [16]. Grain boundaries, in particular random high-angle grain boundaries, can also be effective sinks for radiation defects [17] and extend the low swelling regime to higher radiation doses. Several recent studies using ion irradiation have shown that ultra-fine grained alloys have significant swelling resistance up to 80 dpa as compared to their coarse grained counterparts [18,19]. However, ultra-fine grained alloys tend to have very low ductility [20], which

E-mail address: mericdebelle@wisc.edu (G. Meric de Bellefon).

is undesirable for nuclear reactor applications. Thus, alternative types of internal interfaces such as deformation twin boundaries may be explored for enhancing swelling resistance without compromising ductility.

In austenitic steels, twins may be introduced during annealing, thin film growth, or deformation. Thermo-mechanical treatments can be used to promote the formation of annealing twins in SS [21]. The density of twin boundaries (area of twin boundaries per unit volume) is however low due to the width of annealing twins. A high density of twin boundaries can be achieved with in laboratory-scale thin films produced by processes such as electrodeposition or physical vapor deposition (growth twins) [22], but these processes are not suitable for fabricating components. High densities of twin boundaries can however be achieved in components via deformation twinning (see reviews [23] and [24]). By relying on large strain rate deformation followed by annealing at moderate temperatures (e.g., 700 °C), several studies have demonstrated that high densities of twin boundaries can be achieved while maintaining high ductility levels in SS [25–28].

Deformation twin boundaries are generally  $\Sigma 3$  {111} coherent twin boundaries (CTBs) and occasionally  $\Sigma 3$  {112} symmetric incoherent twin boundaries (ITBs) at locations where the twin has ledges or tips [29]. CTBs are considered as very weak sinks. For example, irradiation experiments showed insignificant or no void-denuded zone in the vicinity of CTBs [30–33] and low or insignificant radiation-induced segregation (RIS) across CTBs as compared to random high-angle grain boundaries [31,34–39]. The weak sink strength is in particular related to the fact that CTBs have a very low free energy among  $\Sigma 3$  (110) tilt boundaries [40]. First-principle simulations of point defect formation

<sup>\*</sup> Corresponding author.

energies and recombination ranges at CTBs in Cu support the experimental observations of their low sink strength [32,41]. However, observations of the radiation response of CTBs reported in the literature are typically conducted on isolated CTBs from wide annealing twins. It can then be hypothesized that the sink effect of an isolated CTB is too weak to be detectable, but that a high density of CTBs could combine to produce a significant sink strength and impact the radiation response. Low-dose ion irradiation experiments of nanotwinned Ag [42–45] and nanotwinned Cu [46] thin films produced by physical vapor deposition [47] support this hypothesis. In this paper, the effectiveness of deformation twin boundaries as sinks for point defects is reported in an ionirradiated SS. It will be shown that regions containing closely-spaced twin boundaries exhibit a higher resistance to void swelling than regions with no twins.

The test material for this study was austenitic 316 SS of the following composition (wt%): 14-Ni, 18-Cr, 3.0-Mo, 0.10-Si, 0.94-Mn, 0.04-C, 0.009-N. A bar of the test material was annealed at 1050 °C for 30 min, water guenched, and cold-rolled with a 30% thickness reduction at room temperature to introduce deformation twins. A bulk sample for irradiation was prepared by cutting a section perpendicular to the rolling direction, polishing it down progressively to 1200 grit surface finish, and electro-polishing it with a standard A2 electrolyte at -15°C for 10 min to remove about 200 µm of materials from the surface, thereby removing all defects induced by mechanical polishing. A control sample was prepared from a non-cold-rolled bar. The electro-polished surface of the bulk sample was irradiated with 3.5-MeV Fe<sup>2+</sup> ions at 500 °C to a fluence of about  $5 \times 10^{16}$  ions·cm<sup>-2</sup> (about 50 dpa at peak damage depth of 1 µm as estimated with SRIM [48]) at a flux of about  $5 \times 10^{12}$  ions·cm<sup>-2</sup>·s<sup>-1</sup>. The ion beam was not rastered to better emulate neutron irradiation [49]. Cross-sectional specimens for transmission electron microscopy (TEM) were extracted from the bulk samples and prepared by focused ion beam (FIB) machining using 30 kV Ga<sup>+</sup> ions followed by 5 kV Ga<sup>+</sup> ions. The FIB instrument was a Zeiss Auriga FIB equipped with a Ga liquid metal ion source and a Schottky field emission scanning electron microscope (SEM). Conventional TEM observations of voids were performed using an FEI Tecnai TF-30 equipped with a Schottky field-emission electron gun operating at 300 kV. Chemical segregation at boundaries was measured using an energydispersive X-ray spectroscopy (EDS) detector attached to an FEI Titan aberration-correct Scanning TEM equipped with a Schottky fieldemission electron gun operating at 200 kV. Electron Back Scatter Diffraction (EBSD) mapping was performed on a FEI Helios G4 UX Extreme High-Resolution Field Emission Scanning Electron Microscope equipped with an EDAX Hiraki Super EBSD camera and the TEAM EBSD data collection software. An accelerating voltage of 30 kV, a current of 26 nA, and a step size of 15 nm were used. The working distance was about 4 mm. Scans were performed using  $5 \times 5$  binning at a rate of ~200 points per second.

The location of the cross-sectional specimen on the surface of the bulk sample from the cold-rolled test material is shown in Fig. 1a and its transmission EBSD map is shown in Fig. 1b. As seen in the micrograph, the specimen has two main grains: one heavily twinned grain on the left and an un-twinned grain on the right. The void distribution was analyzed using the through focus imaging condition [50]. Under this condition, the under-focused images have a dark Fresnel fringe around the voids, the over-focused images have a bright Fresnel fringe around the voids, and the in-focus images show voids with negligible contrast. Better void contrast is usually obtained in kinematical imaging conditions [50]. Under this imaging condition, the background contrast for dislocations and twin boundaries is weak. An example over-focused, kinematical image is shown in Fig. 2a. The same region in in-focus, dynamical imaging condition to reveal twin boundaries at a higher contrast is shown in the rectangle embedded in Fig. 2b.

The main observation from the micrographs is that the void density is strongly affected by the presence of deformation twin boundaries. Some regions with a high density of twin boundaries exhibit full void

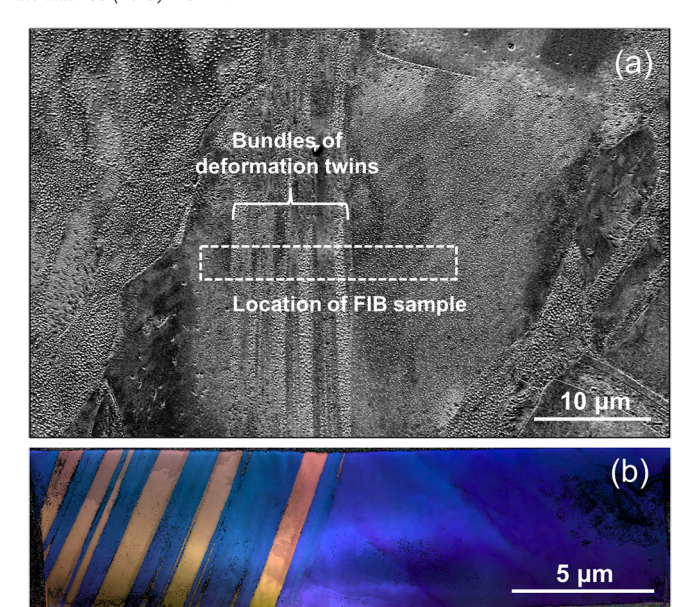


**Fig. 1.** (a) SEM micrograph of the surface of a 30% cold-rolled 316 austenitic stainless steel subject to 3.5 MeV Fe<sup>2+</sup> irradiation at 500 °C to a total fluence of  $6\times10^{16}$  cm<sup>-2</sup>. The location of the cross-sectional specimen used in this study is indicated by the white rectangle. (b) Transmission EBSD map of the cross-sectional specimen shows some large deformation twins on the left grain. The color indicates the crystal orientation with respect to a random direction. (For interpretation of the references to color in this figure legend, the reader is referred to the web version of this article.)

suppression as shown in the center-left and far right regions of Fig. 2a. Some regions with a moderate density of twin boundaries show less pronounced void suppression, which is typically associated with a somewhat degraded deformation twin microstructure likely caused by radiation-induced de-twinning [51]. To quantify the role of deformation twin boundaries on swelling, void swelling was estimated and compared to the local density of twin boundaries. Void swelling was estimated by approximating voids as spheres and measuring the diameters of all voids in regions of interests. Because irradiation was performed on bulk samples, the pre-irradiation twin boundary density cannot be known. However, numerous observations of deformation twins in un-irradiated areas reveal that they almost always run from grain boundary to grain boundary. The density of twin boundaries just below the damage zone (at the top of the un-irradiated zone) was therefore used to estimate the pre-irradiation twin boundary density. In regions with closely-spaced twins, this pre-irradiation twin boundary density is uniform with a mean spacing between twin boundaries of approximately 20 nm. These regions are clearly separated from one another by wide regions with no twin boundary. Void sizes were measured separately for two types of regions: regions with closelyspaced twin boundaries and regions with no twin boundary, as defined by the top of the un-irradiated zone. Using this convention, Fig. 2c shows estimated swelling amounts in these regions. On average, the swelling is reduced by a factor of three in the regions with closelyspaced twin boundaries (0.09% swelling vs. 0.28% swelling). By comparison, swelling in the control, non-cold-rolled material was about 3%. The specimen thickness was measured to be about 150 nm using the Electron Energy-Loss Spectrometry method [52]. The measured thicknesses were similar in regions with and without voids. EDS measurements of chemical concentration across isolated and closely-spaced CTBs showed moderate RIS - about 5 wt%-Cr depletion, as compared to 15 wt%-Cr depletion at a random high angle grain boundary, as shown in Fig. 3.

The driving force for void formation is a supersaturation of vacancies [1]. This supersaturation of vacancies is caused by the formation of vacancies through displacement cascades and the preferential absorption of self-interstitial atoms by dislocations [53]. The evolution of swelling with dose usually occurs in two regimes: a low-swelling transient

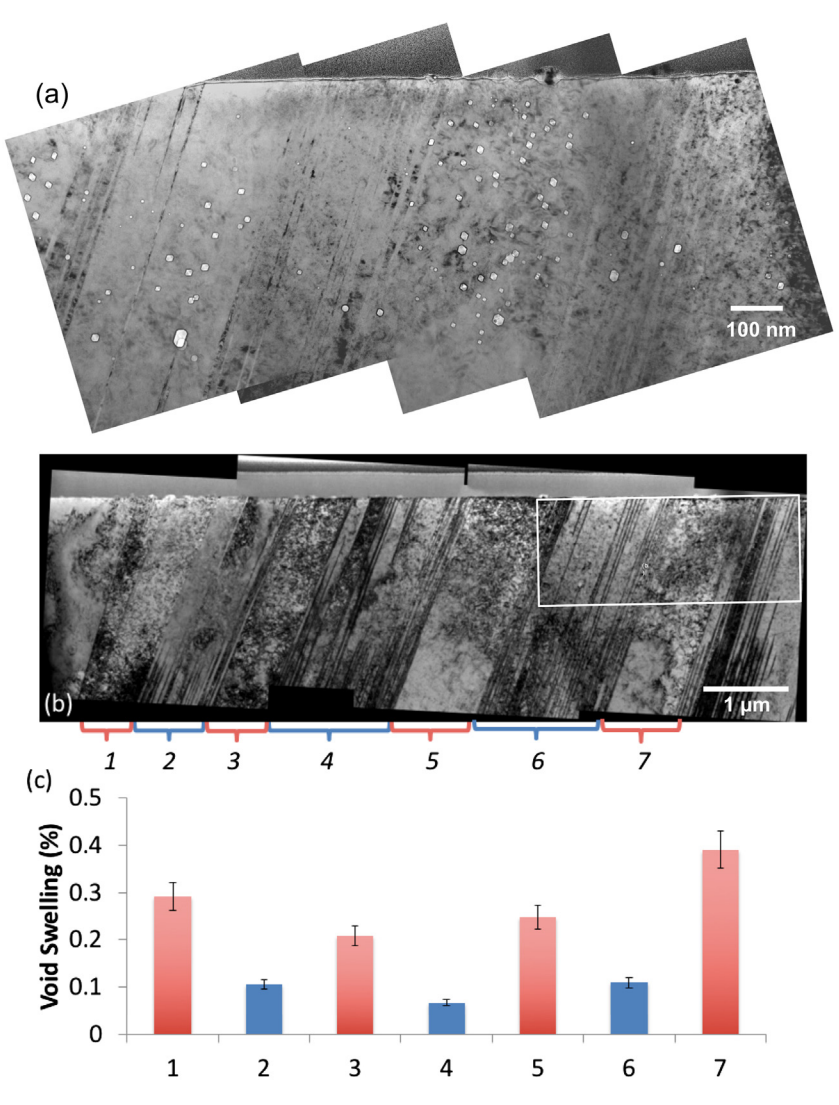
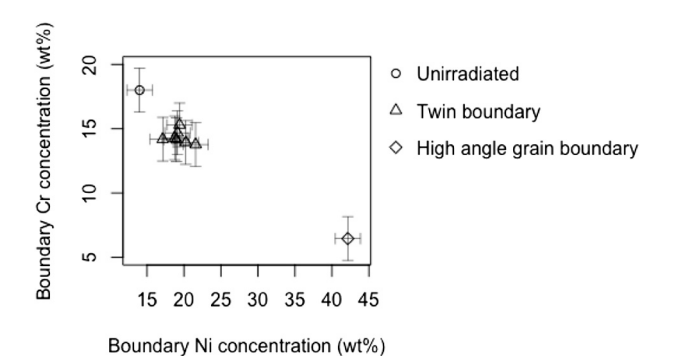


Fig. 2. Void swelling suppression by deformation twin boundaries in the cross-sectional specimen extracted from a 30% cold-rolled 316 austenitic stainless steel subject to 3.5 MeV  $Fe^{2+}$  irradiation at 500 °C to a total fluence of  $6 \times 10^{16}$  cm<sup>-2</sup>; (a) TEM micrograph in over-focused, kinematical imaging conditions to obtain void contrast; (b) TEM micrograph in in-focus, dynamical imaging condition to obtain twin boundary contrast; the boxed region corresponds to the region shown in (a); (c) quantitative analysis of average void swelling in regions with high density of twin boundaries (blue and even numbers) vs. regions with no twin boundary (red and odd numbers). (For interpretation of the references to color in this figure legend, the reader is referred to the web version of this article.)

regime (swelling rate of less than 0.01%/dpa) followed by a high-swelling rate regime (in austenitic steels, swelling rates can be from 0.4 to 1% per dpa for irradiation temperatures between 400 and 600 °C [54–56]). Ion irradiation under the conditions used in the present



**Fig. 3.** Radiation-induced segregation measurements of Cr and Ni concentration at several deformation twin CTBs  $(\Delta)$ , a random high angle grain boundary  $(\diamond)$ , and an unirradiated boundary  $(\diamond)$ . All measurements were performed with STEM EDS at the same depth of 0.6  $\mu$ m in the same cross-sectional specimen as above.

study is expected to follow the same trend albeit with less pronounced swelling and swelling rates, as observed in [18]. Accordingly, the 3% void swelling observed after irradiation in the non-cold-rolled 316 SS is likely in the high-swelling rate regime. In contrast, the overall lower swelling in the irradiated, cold-rolled 316 SS is likely still in the low-swelling transient regime. The apparent decrease in twin boundary density in the irradiated zone as compared to the un-irradiated zone directly below indicates that the twin microstructure may disappear after a long enough irradiation, and that the beneficial role of deformation twins is likely to extend the low-swelling transient regime.

In the studied material, deformation twin boundaries are for the most part  $\Sigma 3$  {111} CTBs. As detailed above, observations of isolated CTBs from annealing twins rarely reveal any void-denuded zone [30–32]. In accordance with the literature, observations in this study of isolated CTBs of annealing twins from the non-cold-rolled 316 SS irradiated under the same conditions did not exhibit any void-denuded zone. However, many examples of complete void suppression were observed within some bundles of closely-spaced CTBs (see Fig. 2a). This can be rationalized using arguments from kinetic rate theory models. In these models, a sink such as a grain boundary can trap mobile vacancies (at 500 °C vacancies can be considered mobile) and induce a gradient in vacancy concentration with a lower concentration close to the

boundary than in the bulk. The presence of RIS (see Fig. 3) indicates the occurrence of a weak sink effect at all individual CTBs. For an isolated CTB, the weakness of the sink effect leads to a vacancy concentration gradient that is not pronounced. As such, the vacancy supersaturation near the boundary remains large and above the critical vacancy supersaturation required for void nucleation. In the case of several closely-spaced CTBs, the probability of vacancy trapping by a CTB is increased. Accordingly, the supersaturation of vacancies in the region near the CTBs decreases enough to be below the critical supersaturation for void nucleation.

The influence of the spacing between CTBs on vacancy supersaturation can be discussed using results from computer simulations. Demkowicz et al. [57] calculated the concentration of mobile vacancies between parallel interface sinks for a varying interface spacing using a 1D reaction-diffusion model in pure Cu. Their results show that for a defect production rate of  $10^{25} \text{ m}^{-3} \cdot \text{s}^{-1}$  (relevant to the present irradiation condition), narrowing the spacing between interfaces considered as perfect sinks from infinitely-spaced to 20 nm reduced the vacancy concentration between interfaces by a factor of about 50. The vacancy concentration is reduced by a factor of 5 for imperfect interface sinks having a sink efficiency (ratio of vacancy flux into that interface to the flux into a perfect sink) of 0.9. The influence of a reduction in the concentration of vacancies on void swelling can be discussed using thermodynamic-based models of void nucleation in Ni from Katz and Wiedersich [58]. The void density in the regions with no twins of the cold-rolled and irradiated 316 SS used in the present study is about  $10^{15}$  cm<sup>-3</sup>, which was obtained after 10,000 s of irradiation. If steady state conditions were reached early in the irradiation, the estimated void nucleation rate is about  $10^{11}\,\text{cm}^{-3}\!\cdot\!\text{s}^{-1}.$  Using Katz and Wiedersich's calculations (plots from Fig. 5 in [58]), the supersaturation of vacancies in these regions is estimated to be between 10<sup>3</sup> and 10<sup>4</sup>. Their plots show that decreasing that vacancy supersaturation by a factor of 5 decreases the void nucleation rate by about four orders of magnitude, i.e., it effectively suppresses void swelling. The observed void swelling suppression can therefore be understood as follows: the 20-nm spacing between CTBs, i.e., imperfect interface sinks, can reduce the vacancy concentration by a factor of 5 as compared to infinitely-spaced CTBs (per Demkowicz et al.), and this reduction in vacancy concentration can suppress swelling (per Katz and Wiedersich).

The influence of a high density of deformation twin boundaries on the void swelling response of an austenitic stainless steel was investigated. It was shown that regions containing a high density of closelyspaced deformation twins exhibit a higher resistance to void swelling than regions with no twins. Using arguments derived from kinetic rate theory models, it can be inferred that the void suppression in regions with closely-spaced twin boundaries is driven by the sink effect of individual CTBs and the narrower spacing between them. The swelling resistance is likely limited by an apparent radiation-induced detwinning that leads the density of twin boundaries to decrease in some regions. In regions where de-twinning seems to have occurred, swelling is still reduced by a factor of three on average as compared to swelling in regions with no twin prior to irradiation. Thermomechanical treatments to generate a high density of deformation twins may provide a design strategy to delay the onset of void swelling in materials exposed to radiation.

### Acknowledgements

This paper is dedicated to co-author Jean Claude van Duysen, who disappeared a few weeks before submission. The authors acknowledge support from the following organizations: for funding of GM, U.S. Department of Energy through an Integrated University Program Graduate Fellowship; for microstructure characterization, the National Science Foundation through the University of Wisconsin

Materials Research Science and Engineering Center (DMR-1720415); for ion irradiation experiments, the Ion Beam Laboratory at the University of Wisconsin, Madison, and its staff Mr. Kim Kriewaldt and Dr. Li He, and the U.S. Department of Energy, Office of Nuclear Energy under DOE Idaho Operations Office Contract DE-AC07-051D14517 through a Nuclear Science User Facilities experimental project.

#### References

- [1] Gary S. Was, Fundamentals of Radiation Materials Science, Springer Berlin Heidelberg, Berlin, Heidelberg, 2007.
- 2] L.K. Mansur, J. Nucl. Mater. 216 (1994) 97-123.
- [3] F.A. Garner, M.B. Toloczko, B.H. Sencer, J. Nucl. Mater. 276 (2000) 123–142.
- [4] S.J. Zinkle, P.J. Maziasz, R.E. Stoller, J. Nucl. Mater. 206 (1993) 266-286.
- [5] S.J. Zinkle, L.L. Snead, Annu. Rev. Mater. Res. 44 (2014) 241-267.
- [6] I.J. Beyerlein, A. Caro, M.J. Demkowicz, N.A. Mara, A. Misra, B.P. Uberuaga, Mater. Today 16 (2013) 443–449.
- [7] M.J. Demkowicz, P. Bellon, B.D. Wirth, MRS Bull. 35 (2010) 992–998.
- [8] W. Han, M.J. Demkowicz, N.A. Mara, E. Fu, S. Sinha, A.D. Rollett, Y. Wang, J.S. Carpenter, I.J. Beyerlein, A. Misra, Adv. Mater. 25 (2013) 6975–6979.
- [9] W.Z. Han, N.A. Mara, Y.Q. Wang, A. Misra, M.J. Demkowicz, J. Nucl. Mater. 452 (2014) 57–60.
- [10] T.R. Allen, K. Sridharan, L. Tan, W.E. Windes, J.I. Cole, D.C. Crawford, G.S. Was, Nucl. Technol. 162 (2008) 342–357.
- [11] C. Cawthorne, E.J. Fulton, Nature 216 (1967) 575-576.
- [12] F.A. Garner, Radiation Damage in Austenitic Steels, 1st ed. Elsevier Inc., 2012
- [13] E.E. Bloom, J.O. Stiegler, J. Nucl. Mater. 35 (1970) 244–246.
- [14] E.H. Lee, L.K. Mansur, Metall. Trans. A. 23A (1992) 1977–1986.
- [15] B.J. Makenas, S.A. Chastain, B.C. Gneiting, LMR A Decad. LMR Prog. Promise, ANS Winter Meet, 1990.
- [16] S.J. Zinkle, G.S. Was, Acta Mater. 61 (2013) 735-758.
- [17] B.N. Slngh, M. Eldrup, S.J. Zlnkle, S.I. Goeubov, Philos. Mag. A 82 (2002) 1137–1158.
- [18] C. Sun, S. Zheng, C.C. Wei, Y. Wu, L. Shao, Y. Yang, K.T. Hartwig, S.A. Maloy, S.J. Zinkle, T.R. Allen, H. Wang, X. Zhang, Sci. Rep. 5 (2015) 7801.
- [19] B. Radiguet, A. Etienne, P. Pareige, X. Sauvage, R. Valiev, J. Mater. Sci. 43 (2008) 7338–7343.
- [20] R. Valiev, Nat. Mater. 3 (2004) 511–516.
- [21] S. Kobayashi, M. Hirata, S. Tsurekawa, T. Watanabe, Procedia Eng. 10 (2011) 112–117.
- [22] I.J. Beyerlein, X. Zhang, A. Misra, Annu. Rev. Mater. Res. 44 (2014) 329–363.
- [23] J.W. Christian, S. Mahajan, Prog. Mater. Sci. 39 (1995) 1–157.
- [24] M. Niewczas, Dislocations in Solids, 13, 2007 263–364.
- [25] S.J. Wang, T. Jozaghi, I. Karaman, R. Arroyave, Y.I. Chumlyakov, Mater. Sci. Eng. A 694 (2017) 121–131.
- [26] F.K. Yan, N.R. Tao, K. Lu, Scr. Mater. 84–85 (2014) 31–34.
- [27] G.Z. Liu, N.R. Tao, K. Lu, J. Mater. Sci. Technol. 26 (2010) 289–292.
- [28] L. Xiong, Z.S. You, S.D. Qu, L. Lu, Acta Mater. 150 (2018) 130-138.
- [29] M.H. Yoo, Chapter 21 Twinning and Mechanical Behavior, 2002.
- [30] W.Z. Han, M.J. Demkowicz, E.G. Fu, Y.Q. Wang, A. Misra, Acta Mater. 60 (2012) 6341–6351.
- [31] C.M. Barr, L. Barnard, J.E. Nathaniel, K. Hattar, K.A. Unocic, I. Szlurfarska, D. Morgan, M.L. Taheri, J. Mater. Res. 30 (2015) 1290–1299.
- [32] M.J. Demkowicz, O. Anderoglu, X. Zhang, A. Misra, J. Mater. Res. 26 (2011) 1666–1675.
- [33] T. Lagrange, K. Arakawa, H. Yasuda, M. Kumar, Acta Mater. 96 (2015) 284–291.
- [34] K.G. Field, Y. Yang, T.R. Allen, J.T. Busby, Acta Mater. 89 (2015) 438–449.
- [35] C.M. Barr, G.A. Vetterick, K.A. Unocic, K. Hattar, X.M. Bai, M.L. Taheri, Acta Mater. 67 (2014) 145–155.
- [36] E.A. Kenik, T. Inazumi, G.E.C. Bell, J. Nucl. Mater. 183 (1991) 145-153.
- [37] N. Sakaguchi, M. Endo, S. Watanabe, H. Kinoshita, S. Yamashita, H. Kokawa, J. Nucl. Mater. 434 (2013) 65–71.
- [38] S.M. Bruemmer, L.A. Charlot, J.S. Vetrano, E.P. Simonen, MRS Proc. 373 (1994) 119.
- [39] S. Watanabe, Y. Takamatsu, N. Sakaguchi, H. Takahashi, J. Nucl. Mater. 287 (2000) 152–156.
- [40] V.V. Bulatov, B.W. Reed, M. Kumar, Acta Mater. 65 (2014) 161–175.
- 41] A. Hallil, A. Metsue, J. Bouhattate, X. Feaugas, Philos. Mag. 96 (2016) 2088–2114.
- [42] K.Y. Yu, D. Bufford, C. Sun, Y. Liu, H. Wang, M.A. Kirk, M. Li, X. Zhang, Nat. Commun. 4 (2013) 1377.
- [43] K.Y. Yu, D. Bufford, F. Khatkhatay, H. Wang, M.A. Kirk, X. Zhang, Scr. Mater. 69 (2013) 385–388.
- [44] J. Li, K.Y. Yu, Y. Chen, M. Song, H. Wang, M.A. Kirk, M. Li, X. Zhang, Nano Lett. 15 (2015) 2922–2927.
- [45] J. Li, Y. Chen, H. Wang, X. Zhang, Metall. Mater. Trans. A Phys. Metall. Mater. Sci. 48 (2017) 1466–1473.
- [46] C. Fan, J. Li, Z. Fan, H. Wang, X. Zhang, Metall. Mater. Trans. A Phys. Metall. Mater. Sci. 48 (2017) 5172–5180.
- [47] D. Bufford, H. Wang, X. Zhang, Acta Mater. 59 (2011) 93-101.
- [48] J.F. Ziegler, M.D. Ziegler, J.P. Biersack, Nucl. Instrum. Methods Phys. Res., Sect. B 268 (2010) 1818–1823.
- [49] J.G. Gigax, E. Aydogan, T. Chen, D. Chen, L. Shao, Y. Wu, W.Y. Lo, Y. Yang, F.A. Garner, J. Nucl. Mater. 465 (2015) 343–348.
- [50] H. Wahid, S. Ahmad, M.A.M. Nor, M.A. Rashid, J. Ekon. Malaysia 51 (2017) 39-54.

- [51] Y. Chen, H. Wang, M.A. Kirk, M. Li, J. Wang, X. Zhang, Scr. Mater. 130 (2017) 37–41.
  [52] D.B. Williams, C.B. Carter, The Transmission Electron Microscope, 2009.
  [53] A.D. Brailsford, R. Bullough, J. Nucl. Mater. 44 (1972) 121–135.
  [54] F.A. Garner, H.R. Brager, J. Nucl. Mater. 133–134 (1985) 511–514.
  [55] F.A. Garner, H.R. Brager, J. Nucl. Mater. 155–157 (1988) 833–837.

- [56] R.E. Stoller, P.J. Maziasz, A.F. Rowcliffe, M.P. Tanaka, J. Nucl. Mater. 155–157 (1988)
- [56] K.E. Stöller, P.J. Maziasz, A.F. Rowellie, W.F. Taliaka, J. Nucl. Match. 153–157 (1566) 1328–1334.
  [57] M.J. Demkowicz, R.G. Hoagland, B.P. Uberuaga, A. Misra, Phys. Rev. B: Condens. Matter Mater. Phys. 84 (2011) 1–5.
  [58] J.L. Katz, H. Wiedersich, J. Chem. Phys. 55 (1971) 1414–1425.